Biophysical and Structural Characterization of DCC 3-5 and Netrin-1 Binding Interaction

By

Haben Gabir

A Thesis submitted to the Faculty of Graduate Studies of

The University of Manitoba

In partial fulfilment of the requirements of the degree of

MASTER OF SCIENCE

Department of Chemistry

University of Manitoba

Winnipeg

Abstract

Deleted in Colorectal Cancer (DCC) is a transmembrane receptor that belongs to the immunoglobulin superfamily. Its function as a dependence receptor makes DCC a tumour suppressor in colorectal cancer. Its primary ligand is Netrin-1, a chemotropic soluble protein responsible for attractive and repulsive migration of axon growth tips during neural development. Netrin -1 and DCC are also play significant roles in cell migration, proliferation, differentiation and apoptosis in other tissues.

DCC has two splice variant whose functional difference or binding sites with netrin-1 are not fully known. In this project, to better understand the mechanism of interaction between DCC and Netrin-1, We focused on using an integrated approach of biophysical and structural biology techniques to characterize DCC and DCC with Netrin-1 bound in solution. Both DCC and Netrin-1 were expressed in mammalian cells and purified by affinity chromatography and Size exclusion chromatography (SEC). The proteins were then characterized by Analytical Ultracentrifugation to determine the stability, dispersion, and behaviour in solution, as well as to confirm complex formation. Further characterization was done by SEC-Small Angle X-ray Scattering (SEC-SAXS) to generate low resolution models. The SEC-SAXS models were made Ab initio using the ATSAS data analysis software package and Density in Solution Scattering electron density determination algorithm. The models showed that the DCC variants to be long flexible proteins that when bound to Netrin-1 make a stable complex. When comparing the Netrin-1 complexes with the DCC variants, the larger and longer DCC was more stable, suggesting the additional components had an effect of binding. Final DCC alone and Netrin-1

with DCC were crystallized to build high resolution models. A 2.6A crystal structure of DCC was built that corroborated the SEC-SAXS models.

Acknowledgement

I could not have asked for a better supervisor and mentor then Dr. Jorge Stetefeld. His persistence to providing the best environment for learning and pursuing research has made my continued stay at the university some of my best years. His constant encouragement and support have allowed me to dream of futures I never thought possible.

I would like to thank Drs. Markus Meier, Aniel Moya Torres, Matthew McDougall and Monika Guptra for their friendship and continued assistance in my education and training. They held my hand through many tough learning curves until I was comfortable enough on my own.

For their patience, assistance and invaluable input, I am forever grateful to my committee members Dr. Gerd Prehna, Joe O'Neil and Rebecca Davis.

Table of Contents

List of Tables

Table of Figures

Introduction

Protein- Protein Interactions

Protein - protein interactions (PPI) are key for cell to cell communication, cell response to environmental changes and proper tissue function. Secreted proteins, through PPI, will relay messages between cells through receptor activation and signal amplification. Specifically, in nervous system development, PPI facilitates the migration of axons via signalling molecules called guidance cues[6]. In responses to the cues, the tips of the axon reorganize their cytoskeleton and migration occurs[1].

Guidance Cues and Neuronal Development

Through their specialized tips, called growth cones, axons can integrate signals from guidance cues to affect their direction of migration and elongation. Several diffuse, membrane bound or matrix coated ligands, through PPI, control axon elongation in a specific direction[2]. To date, four major families of canonical guidance cues are known: Netrins, slits, semaphorins and ephrins., a guidance cue that shares no homology with the canonical cues called draxin was recently identified [3]. Growth cones are attracted or repelled in direction from the concentration gradient of the signalling molecule. They also vary in the range of their effect, where some have short range and contact mediated interactions, others are long range diffusion mediated cues[4].

Short range signaling molecules include the transmembrane cell adhesion molecules and assembled proteins of the extracellular matrix such as laminin and fibronectin. These proteins provide roadways for the growth cones to travel on[5]. Other cues such as netrin and slit proteins are diffused in the matrix and will, as a function of their receptors, illicit an attraction or repulsion signal. Initially, guidance cues were thought to have one positive or negative function,

but more research has shown that some proteins, in the netrin family for example, will be bifunctional and will be both attractive and repulsive to growth cones.

Growth cones

The growth cones can migrate and change directions only as a function of their cytoskeletal organization and reorganization. Each cone is separated into three zones, the Central (C) domain, the Peripheral (P) zone and the Transitional (T) zone (A). The C domain contains stable bundles of microtubules that function as support but also as the highway between the cone and the main cell body. The P zone contains the dynamic cytoskeleton of actin bundles that make up the finger-like filopodia. Finally, the T zone between C and P zones controls the penetration of MT into the P zone. The filopodia tips first binds to guidance cues and, through signal transduction, moves and elongates the axon by dynamically building and reorganizing the MT and F-actins[5]. After reaching their targets, growth cones innervate and form a synapse[6].

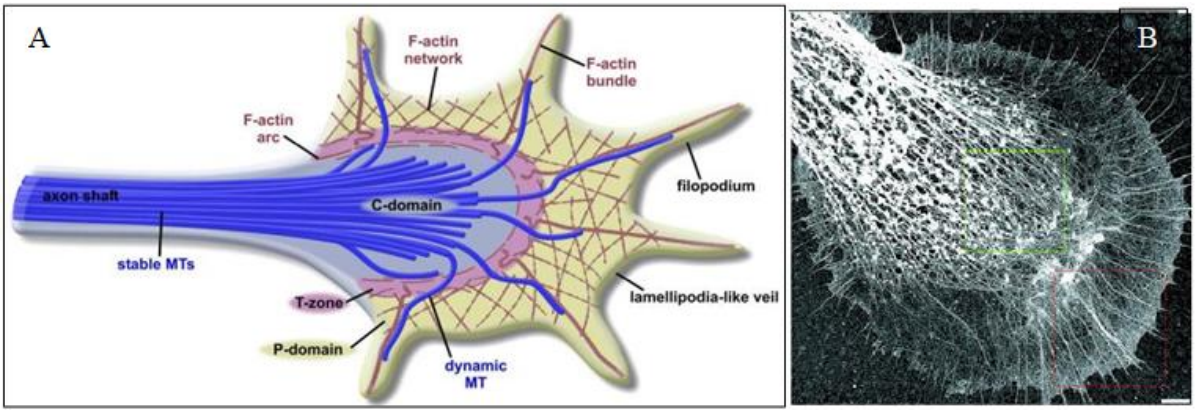

Figure 1: (A) A schematic structure of growth cone showing the Central domain, Peripheral(P) and the transition (T) zone. Each zone serves as the highway between the growth cone and the cell body, the site of cue binding and cytoskeleton reorganization and transition between the two, In blue are the stable microtubules and in red are F-actins proteins. (B) Low magnification rotary shadow electron micrograph of cell growth cone cytoskeleton. Bar, 3.5 um.[7] Used with Permission

Netrin-1 and its Receptors

[8]Netrin-1 was first identified in nematode worm Caenorhabditis elegans in screening of neural development regulator proteins as uncoordinated 6 (Unc6)[9]. It was observed that loss of the homologous gene unc-6/netrin-1 resulted in uncoordinated movement of the worms and misguidance of commissural axons during midline crossing. Now it is understood that in nervous system development netrin -1 is responsible for guiding commissural axons toward the basal structure of the spinal cord (Figure 2)[10]. Commissural axons are axons that connect two different regions in the nervous system. Netrin-1/Unc6 is found in many vertebrates and invertebrates and is highly conserved[11].

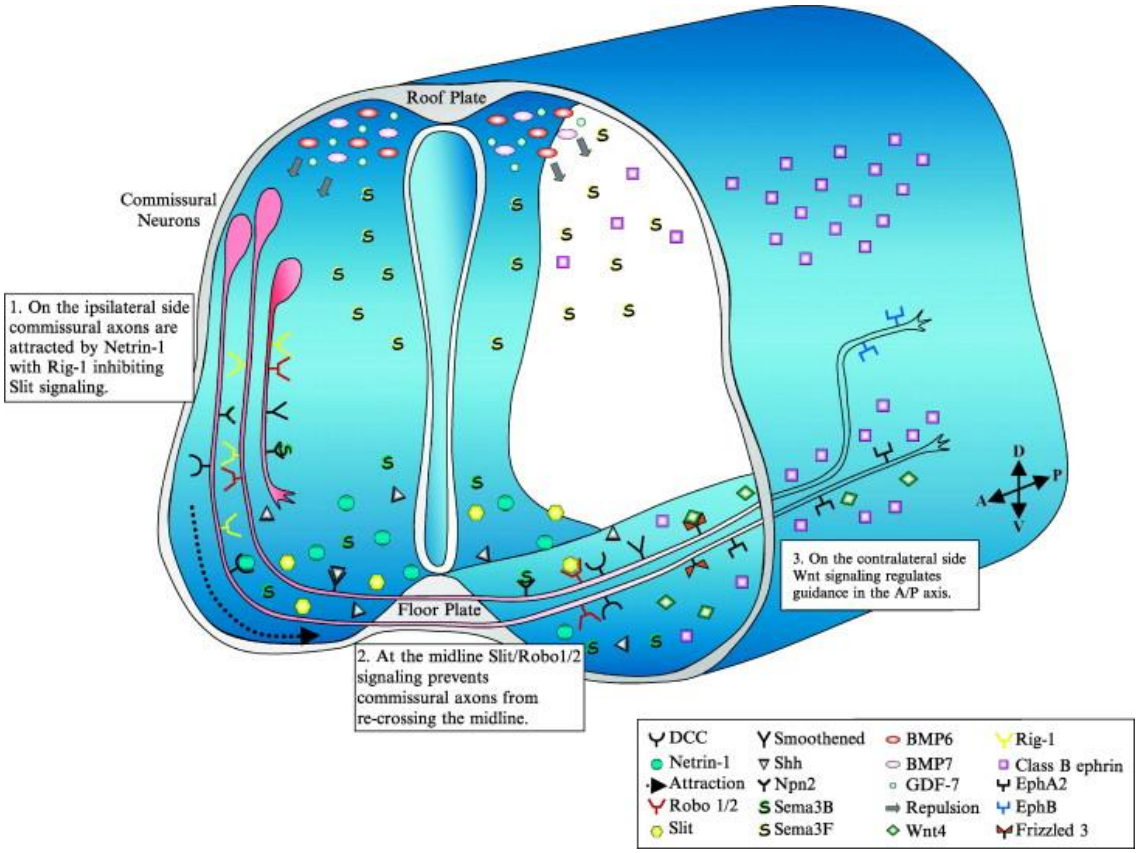

Figure 2: Netrin-1 guides neurons to elongate and migrate their commissural axons from the roof plate ventrally to the floor plate. *Used with Permission*

\Netrin-1 is a member of the Netrin family, a subclass of the Laminin related family and is made up of four soluble diffuse netrins: Netrin-1, -3, -4, and -5, and two carboxy-terminal glycophosphosphatidylinositol tail bound Netrin- G1, and G2, though sequence difference from netrins 1 to 5 suggests Netrin-G1, and G2 evolved separately[12,13].

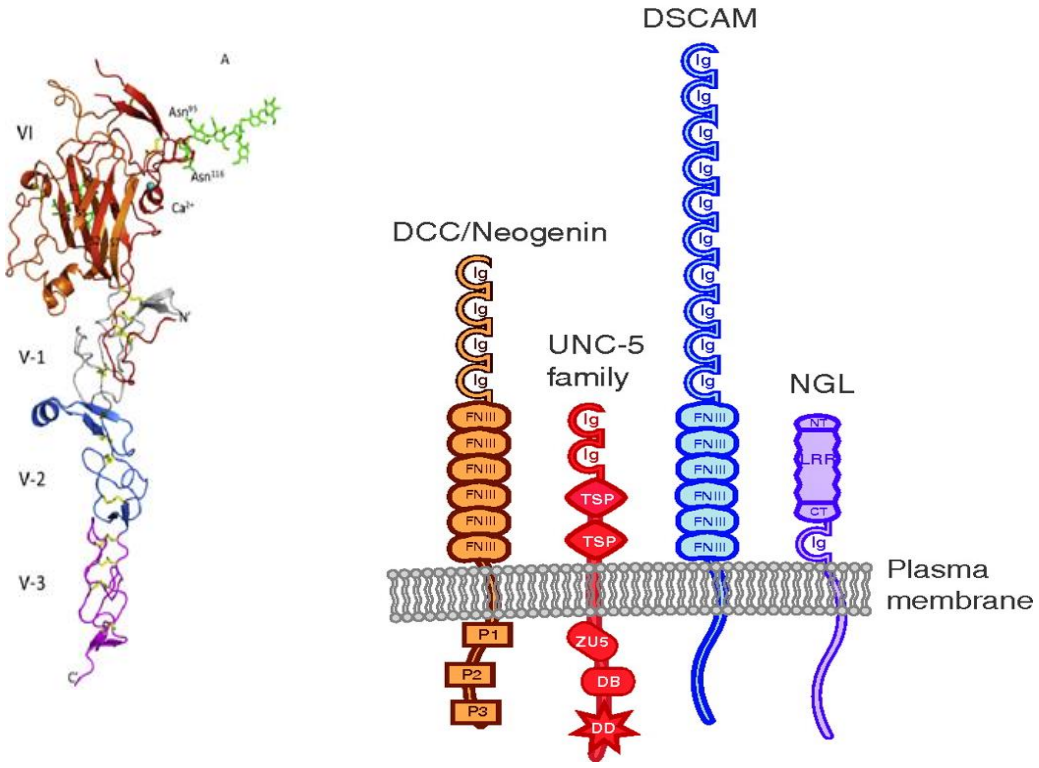

Figure 3: Crystal structure of Netrin-1 with truncated C domain, schematic diagrams of Netrin-1 receptors[1,10]. Used with Permission

Netrin-1 is a 67.5 kDa glycosylated protein. It has 589 residues and is composed of 5 domains. The 5 domains are an N-terminal domain VI, followed by three laminin-type epidermal growth factor (EGF) repeats (V-1, V-2, and V-3) and a positively charged C-terminal domain (domain C). Netrin-1 has 4 N linked glycosylation sites (Figure 3)[10]. Netrin -1 receptors in mammals include Deleted in Colo-rectal Cancer (DCC), DCC paralogue Neoginin, four Uncoordinated 5 (UNC5 (A-D)) and Down Syndrome Cell Adhesion Molecule (DSCAM)[14].

DCC and UNC5 are part of the dependence receptor family. Such receptors are biologically active with or without ligand binding. When bound, they propagate several signals but when unbound they will induce cell death by apoptosis. Therefore, Netrin-1 will be a survival factor in diverse contexts[15],[16].

Deleted in Colorectal Cancer (DCC)

DCC was first identified as a candidate tumour suppression gene and when mutated lead to colorectal cancer. In line with the function of Netrin-1, mutations in DCC also caused congenital mirror movement, where impairment of proper axon growth during development led to voluntary movements performed on the right or left side of the body to be mirrored involuntarily by the opposite side.

DCC is a single pass transmembrane receptor with four N-terminal Ig-domains and six type-III fibronectin domains (FN III) at the extracellular portions[17]. The four Ig-domains form a conserved horseshoe-like conformation by folding back on each other[18]. The FN III domains are the site of Netrin-1 binding. Each DCC has a single pass transmembrane helix followed by conserved cytosolic domains called P1, P2 and P3. These domains dimerize or hetero-dimerize with other receptors netrin-1 binds to.

Neogenin shares approximately 50% sequence similarity with DCC. Neogenin also share the same domain organisation as DCC, which includes the four Ig-domains, six FN III domains and a single pass transmembrane helix connecting the P1-P3 cytosolic domains. Like DCC, neogenin also mediates an attraction response to Netrin-1 concentration gradient when

unbound to UNC5. The high degree of similarity in structure and function, as well as studies in chicken axon guidance cues suggests that neogenin may act as a substitution for DCC[19].

Uncoordinated 5 (UNC5)

While DCC homodimer causes attraction towards a Netrin-1 concentration gradient, UNC5 receptor heterodimerizing with DCC will be repelled by Netrin-1 binding[20]. UNC5 is a member of the Immunoglobulin (Ig) superfamily and has 4 orthologues: UNC5A to D. All four orthologues are composed of two N-terminal Ig-domains, followed by two thrombospondin (TPS) type I domains are then connected through a transmembrane helix. The intracellular domains are composed of a ZU-domain, the DCC-P1 binding domain UPA and a death domain[21].

Down Syndrome Cell Adhesion Molecule (DSCAM)

Located on chromosome 21, DSCAM Human DSCAM (Fig. B) is composed of nine N-terminal Ig-domains, separated by four fibronectin domains from the tenth Ig-domain and followed by two more fibronectin domains. Through a transmembrane domain the cytosolic part is connected DSCAM is expressed by commissural axons of the spinal cord[22]. Upon binding to netrin-1 it can mediate a positive turning response guiding the migrating growth cone through the ventral midline[23]. It was also demonstrated that DSCAM can form receptor complexes with DCC through their ectodomains or transmembrane domains, but unlike DCC homo- or hetero-dimerization with UNC5, not through the cytosolic domains

Netrin Pathway and Cancer

In many cancers, netrin-1 expression levels are significantly changed. In a study of metastatic breast cancer tumour tissues, Netrin-1 was overexpressed in 31.5% of the tissues

tested, by over 5-fold[24]. In brain tumours and neuroblastomas, the expression of human NTN1 is markedly reduced or absent in ~50% and missense mutations were found in one neuroblastoma. NTN1 also expression levels are also reduced in prostate cancers[25].

Aside from netrin-1, Deletions or mutations of DCC and UNC5 are reported in certain cancers. This is because Netrin-1 negatively regulated DCC and Unc5 induced apoptosis and p53-dependant apoptosis. In the intestine epithelium, Netrin-1 is expressed and a gradient from the base to the tip of the villi is formed. DCC expressing cells, when bound Netrin-1, differentiate or proliferate depending on position of the cell on the gradient while cells outside the Netrin-1 gradient at the tip of the epithelial villi undergo apoptosis. Mutations and deletions in DCC cause cells to be insensitive to DCC induced apoptosis. Overexpression of Netrin also confers the same insensitivity to DCC-induced apoptosis. Both cause uncontrolled cell growth and colorectal carcinoma[26].

A specific variant of UNC5, UNC5B, is a transcriptional target of p53, an apoptosis inducer. When netrin-1 is bound to UNC5B, p53 can be stably expressed and accumulated, but is functionally inactivate. In tumour cells, complete loss or reduced UNC5B expression, promotes tumour growth by inhibiting specifically p53-induced apoptosis. This reduction or complete loss of expression was observed in 93% of colorectal tumours, 88% of ovarian tumours, 81% of renal tumours, 74% of lung tumours, 68% of stomach tumours, 49% of breast tumours and 48% of uterine tumours[27].

Netrin-DCC structures

Prior structures of Netrin-1 + DCC FN III 4-5 short and Netrin-1 bound to DCC FNIII 5-6 have previously been published. The two structures both show different binding configurations.

The first structure published, PDB code 4URT, showed binding at V1/EGF-1 with FNIII 5 mediated by sulfate binding. In addition, it shows a crystal mate binding at Site2: with V3/EGF-3

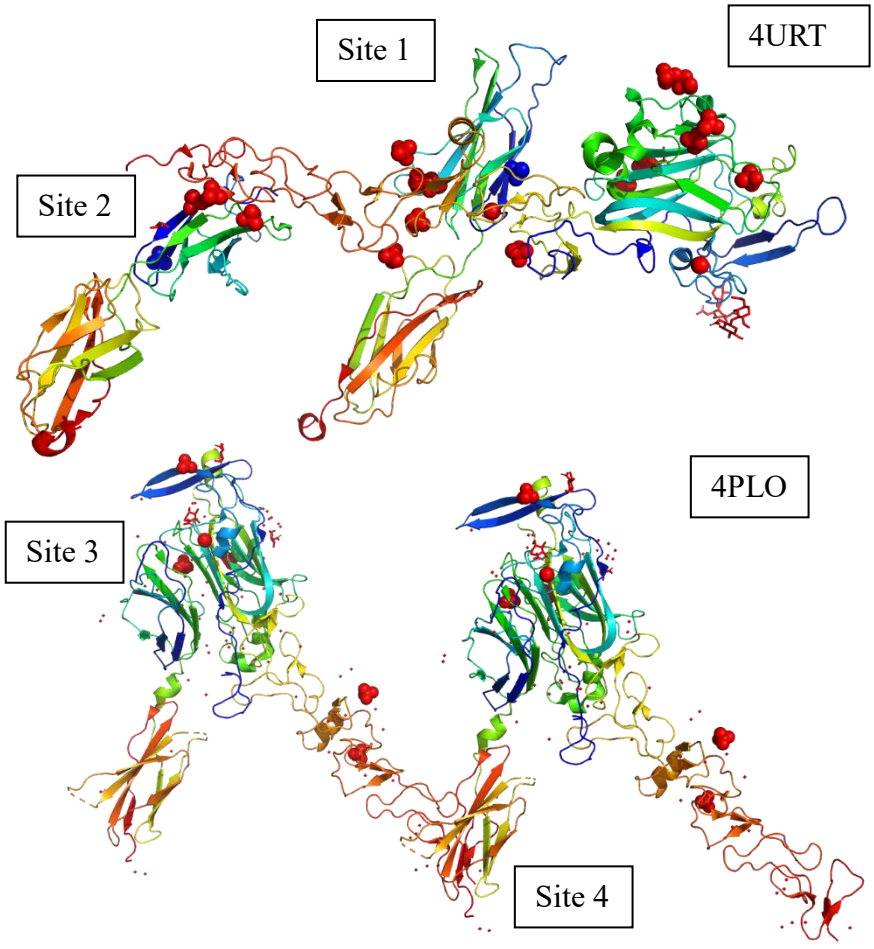

Figure 4: Previously published structure of Netrin-1+DCC. PDB codes 4URT and 4PLO show different binding interactions. 4URT has 2 binding sites at netrin-1 domain V-1 with DCC FN-4 and netrin-1 domain V-3 with DCC FNIII 4, where as in 4PLO, netrin -1 domain VI bind to DCC FNIII 5 and domain V-3 binds with FNIII 6. [28,29]

with FNIII 5, also mediated by sulfate salts[28]. A recent study and structure PDB code 4PLO showed different binding sites where V domain was bound to FNIII 5 and V3/EGF-3 with FNIII 6[29]. Aside from the use of sulfate to mediate the interactions, 4PLO and 4URT do not have any binding sites. Because if conflicting report, it is important to determine the structures using the same Net-1 construct and DCC construct that includes more FNIII domains.

Aim of the Study

The goal of this study is to characterize the binding interaction of Netrin-1 and DCC and to characterize the differences between the DCC variants using an integrated structural and biophysical approach. By coupling X-ray crystallography and Small angle x ray scattering with analytical ultracentrifugation, we can gain information on both the kinetic and structural information of the Netrin-1 DCC interaction. By building a complex of Netrin-1 and longer DCC constructs that include both variants, we can determine the true binding site(s) and finding the difference between the DCC constructs in terms of binding to Netrin-1.

Materials and Methods

Recombinant protein expression and purification

C -terminal Strep-Tag fused chicken Netrin-1 with a deleted C domain (Net1), mouse DCC short Fibronectin-like type III domains 3-5 (DCC short) and mouse DCC long Fibronectin-like type III domains 3-5 (DCC long) DNA fragments were transfected into HEK293T cells ([HEK 293T/17] ATCC® CRL-11268) by Sleeping Beauty plasmids. These transfections were done by Dr. Manual Koch and his group in the university of Cologne, Köln Germany. The cells were shipped to Winnipeg Manitoba in Dulbecco's modified eagle medium (DMEM) (Invitrogen, Waltham, MA, USA). They were subsequently maintained at 37°C in a 5% CO_2 atmosphere. The cells were grown in 10 mL DMEM containing 5% fetal bovine serum (FBS) in polysterol cell culture flasks with a surface area of 75 cm^2 (T75). Some of the cells were grown until confluent then, in 90% FBS and 10% v/v DMSO, were frozen in liquid nitrogen. The other cultures were screened for subclones with a high level of protein expression, and fast growth rate to produce proteins with consistent post-translational modification. Dot-blot westerns were used to qualitatively check the protein expression level via anti-strep antibody coupled to horseradish peroxidase. Clones with the highest proteins production were selected for passaging into polysterol cell culture HYPERflask™ with a surface area of 1720 cm^2 for higher protein production. In the HYPERflask, cells were incubated at 37°C for 48 hr in DMEM containing 2.5% FBS and 1 ug/mL Doxycycline. The supernatent was collected, filtered and frozen in 20^{o}C until protein is needed.

Protein Purification and complex formation

The supernatent was harvested, filtered and passed through strep-tactin affinity column and eluted by 50 mM Tris pH 8, 500 mM + Desthiobiotin and measured by a spectrophotometer

at 280 nm. The eluted proteins were dialyzed in 50 mM Tris pH 7.5, 200 mM NaCl before strep - tag cleavage with bovine thrombin. After strep-tag removal Netrin, DCC short and DCC long weighted 49.50 kDa, 38.75 kDa and 37.67 kDa respectively. Thrombin was removed by passage the solution through a benzamidine serine protease affinity column (GE healthcare). Purity and homogeneity of the thrombin digested protein was assayed by 8% SDS-PAGE and the pure protein was stored at 4°C at 1 mg/mL or less until required. Each protein was applied to a Superdex 200 SEC column (GE Healthcare) equilibrated with 50 mM Tris, pH 7.5, 200 mM NaCl at room temperature. The purified proteins were used for crystallization trials, sent to Diamond UK for Small -angle x ray scattering (Bio-SAXS) or analytical ultracentrifugation (AUC) experiments.

Complexes with netrin, DCC short or DCC long were formed by first SEC purifying the individual proteins, then combining the fractions with a single peak. The receptors were then mixed 1:1 molar ratio and dialysing at room temperature in 50 mM Tris pH 7.5, 200mM NaCl overnight.

Analytical Ultracentrifugation (AUC)

Analytical Ultracentrifugation is a biophysical technique used to characterize proteins in their native buffer condition by looking at the protein behaviour under high centrifugal force[30,31]. It is a robust and non-destructive tool that uses Sedimentation Velocity and Sedimentation Equilibrium to understand the molecular mass, shape, stoichiometry, interaction of the macromolecules, and the association constants of the interactions[32]. This information gives a better understanding of how the DCC and Net1 self interact and, and how they interact with each other.

High concentrations of DCC short and long, 1.85 and 1.45 mg/mL each, were measured at 299 nm wavelength, while low concentration, 0.5 and 0.8 mg/mL were measured at 287 nm. The experiments were measured at 42000 rpm, 144 scans in 24 hours at 20^{o}C. The scans were analyzed using UltraScan III[33]. The analysis used parametrically constrained spectrum analysis to fit the Lamm equations (eq. 1), using a straight-line function to calculated the non-negative least squares fit of the lamm equation[34]. The lamm equation (Equation 1)describes the sedimentation (s) and diffusion (D) of a particle in a sector-shaped cell as a centripetal force is applied. The t, r, c and ω represent the time of sedimentation, radius of the cell window measured, solute concentration and the rotor angular velocity.

The density of the 50 mM Tris pH 7.5, 200 mM NaCl (1.0079 g/cm^3) and viscosity (1.03173 cP). The software also calculated the partial specific volumes (DCC long: 0.7252 cm^3/g, and DCC short: 0.7259 cm^3/g) of each analyte based on the amino acid sequences automatically.

$$\frac{dc}{dt} = \frac{1}{r}\frac{d}{dr}\left[rD\frac{dc}{dr} - s\omega^2 r^2 c\right]$$

Equation 1: Lamm equation which describes particle sedimentation as in an AUC cell

Biological Small Angle X-ray Scattering

Low resolution models of the proteins in aqueous conditions were produced by Biological Small Angle X-ray (Bio-SAXS) and analysed by ScÅtter™, ATSAS package and DENsity from Solution Scattering (Denss) Ab initio electron density determination program. Individual

data sets were collected at the Diamond light source beamline 21 with Eiger 4M detector as each fraction eluted from the Superdex 200 column. The SEC purified DCC long, DCC short, Net+DCC long, Net+DCC short were approximately 3 mg/mL in 50 mM Tris, pH 7.5, 200 mM NaCl buffer when measured. The buffer subtraction and data processing were done using ScÅtter. The radius of gyration (Rg) and maximum particle dimension (Dmax) were calculated using the GNOM program as part of the ATSAS package[35]. Multiple Ab initio models were generated from GNOM output using DAMMIF then the models are averaged, aligned and any model that falls 1 standard deviation outside the consensus was removed and a reference model was generated with the passing models using the DAMAVER program. Finally, DAMMIN, a program that relies on temperature-dependent simulated annealing generated a final refined model and goodness of fit parameter (χ^2) was calculated to assess its quality[36]. While the DAMMIF/DAMAVER/DAMMIN generated ab initio models using dummy atoms to produce a scattering profile that fits the experimental scattering[37], Denss generated models by first making a 3D array of grid points with voxels of prescribed sizes as shown as 2D in Figure 5. Each voxel contains randomly generated electron density and 3D reciprocal space structure factors with phases and amplitudes. The electron densities are converted to intensities by forward Fourier transform, then spherically averaged to simulate a SAXS data collection as the sample is tumbling in solution. The averaged intensities are compared to the experimental data and scaled. After scaling, in the real space, the new electron density maps are constrained with a shrink rapped that flattened the area outside an electron density threshold and removes maps

that are discontinuous. The algorithm cycles between the real space and reciprocal space iteratively until there is no change in the goodness of fit parameter[38].

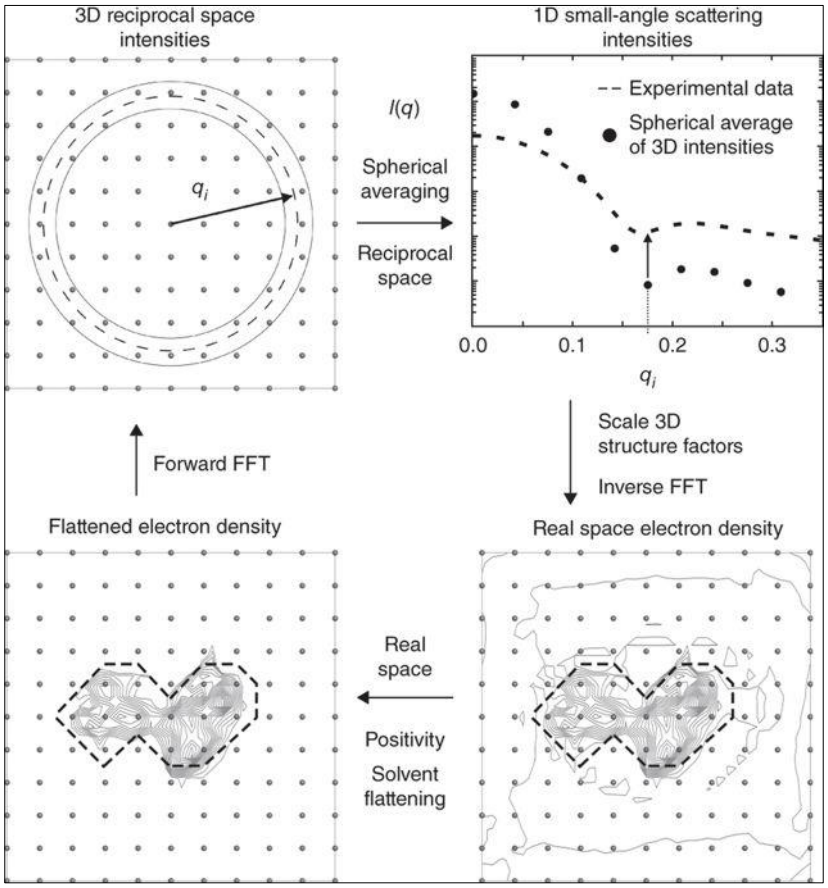

Figure 5: The Method of Denss algorithm to calculate an electron density based on the experimental scattering data. Used with Permission

Crystallization trials

To identify suitable conditions for crystallization of the receptors and the complexes crystallization trials were conducted using commercial crystallization kits: Index, Netrix 1+2, JBS Classic 1-8, JCSG ++1-++4, Jena half block and HR2-117-112 from Hampton Research (CA, USA). The receptors and complexes were purified by SEC as described in the Protein purification

section of this thesis and concentrated to 10 mg/mL to 13 mg/mL before pipetting into the crystallization conditions as sitting drop and vapour diffusion method. The drops were composed of 0.6 µL of the species to be crystallized and 0.6 µL of reservoir solution in 96-well plates. Each well contained 50 µL of reservoir solution. The plates were covered with clear protective film, incubated at 20 °C and monitored for crystal formation.

Diffraction Data collection and Refinement trials

To determine if the crystal hits were protein or salt, they were viewed under a UV microscope. The protein crystals were first diffracted in house using RIGAKU RAXIS V$++ Detector and MicroMax™007 HF X-ray source with the assistance of Dr. Aneil Moya Torres. To improve and increase the quality of diffraction data collected, crystals were refined by hand and sent to beamlines in Saskatoon at the Canadian Light Source, or to the Advanced Photon Source in Chicago, Illinois in the appropriate cryoprotectant. The data produced were processed using XDS[39], the Collaborative Computational Project No. 4 software suite[40] then phased and refined using Phenix software suite. The model building was done in Coot[41]

Results and Discussion

Cell Culture and Protein production

Cells were diluted to 1 cell/100µL and grown for 1 week or until confluent. cells were induced to produce DCC short (figure 7A) and DCC long (figure 7B) before a western dot blot was used to select the highest strep-tagged protein producing cell. After selection and freezing cells, a hyperflask production was started to produce ~600 mL of supernatant with protein. A western was done to confirm protein production of the initial collections (Fig7 A, B). DCC short and DCC long were present in the hyperflask collections with the indicated green band in figure 7B. Note, DCC short and long will smear in buffer conditions with 500 mM NaCl or higher, which includes the media supernatant where Tris and NaCl is added prior to running on a gel. to ensure all strep-tagged protein was collected during strep-tag affinity column purification, a gel was run with the eluted DCC short, the buffers used to wash the column to remove non-specific binding and the hyperflask collection after second pass. The gel showed almost all DCC short was collected after initial pass, note that the largest band on figure 7C lane 4 is the FBS band.

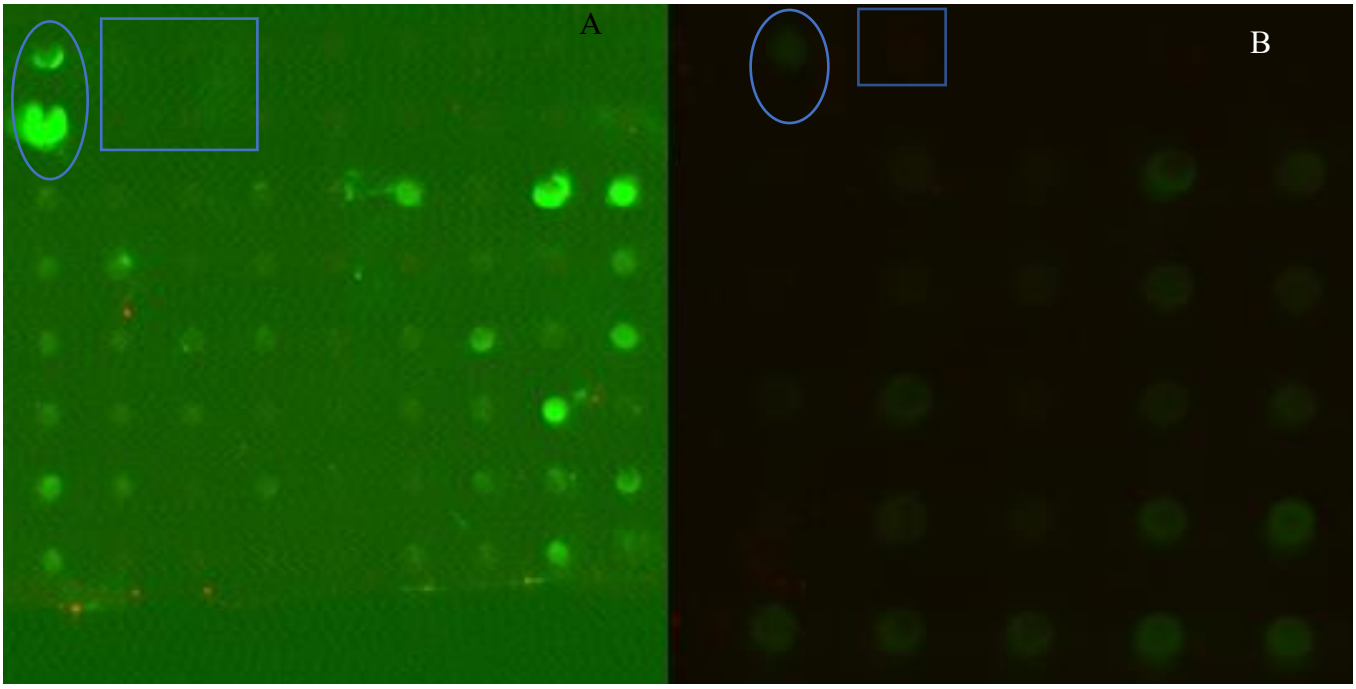

Figure 6: Dot blots of DCC short (A) and DCC long (B). Blue oval outline are the positive controls with uncleaved Net-1 and the blue squares are negative controls of cleaved Net-1, the remaining spaces are buffer and wash solution controls. Cells were diluted in 1cell/ 100µL of DMEM. Cell were grown 37°C in a 5% CO^2 atmosphere until confluent then induced protein production by adding 1ng/mL Doxycycline before performing a dot blot. After clonal selection the cells were frozen with 90% FBS and 10% DMSO in liquid nitrogen. When needed cell cultures were upscaled for higher protein production in HYPERflask. Net1 cell selection was done by Monika Gupta and Dr. Aneil Torres and not included in this thesis.

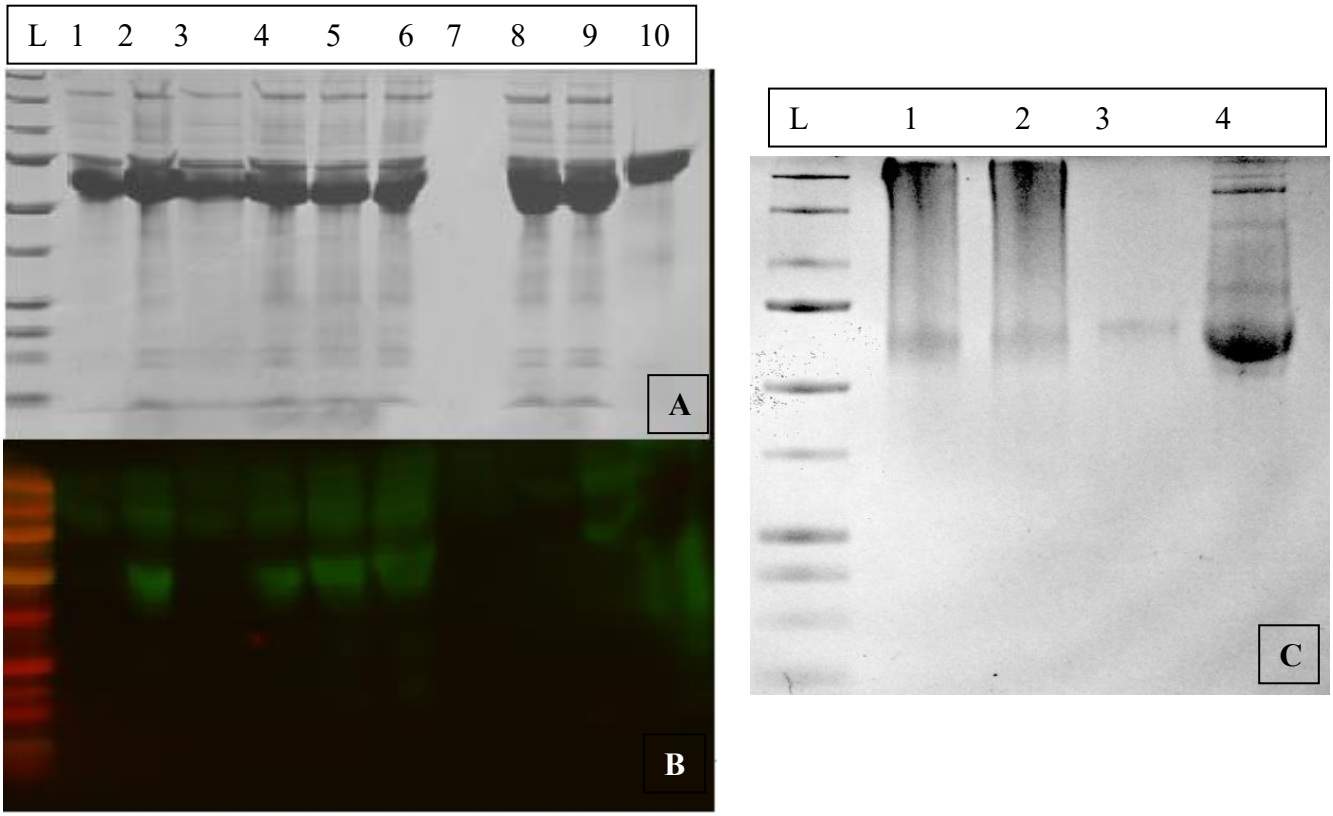

Figure 7: SDS-PAGE(A)and Western blot (B) of DCC short and DCC long, SDS-PAGE (C) of DCC short Collection 1

Gels A and B

Lane 1: DCC short collection 1,

Lane 2: DCC short collection 2,

Lane 3: collection 2 post purification,

Lanes 4-6: DCC short collection 3-5,

Lane 8: DCC long pre-Doxycycline induction,

Lane 9: DCC long collection 1,

Lane 10: positive control Net-1

Gel C

SDS-PAGE (C) of DCC short Collection 1

Lane 1 and 2: DCC short elution

Lane 3: washing buffer 50 mM Tris pH 8 500 mM NaCl

Lane 4: Hyperflask collection 1

Size Exclusion Chromatography profiles

To analyze the binding interaction between Netrin-1 and DCC and to understand the change in binding an additional 20 amino acid linker produces, the receptors with FNIII 3-5 and netrin-1 with a deleted C terminus were produced and processed. The complexes were prepared in 50 mM tris pH 7.5, 200 mM NaCl and purified on a 25 mL Superdex 200 10/300 size exclusion column. DCC short eluted as 2 peaks at 13.17 mL and at 14.28 mL (figure 8A black), suggesting that two species of DCC short exist, though peak 1 is significantly smaller in 280 nm absorbance. Netrin-1 similar elution profile, 2 peaks at 11.77 mL and 13.26 mL elution volume (figure 8A green). From previous unpublished studies done by the Stetefeld group it is known netrin-1 exists in a monomer-dimer equilibrium. The elution of DCC short (Figure 8B black) also suggests a monomer-dimer equilibrium, but that monomeric DCC short may be the predominant form. The peak with the highest absorbance is at 10.64 mL of Net-1+DCC short elution but aggregation is present in solution shown by the peak in the void volume at 8.8 mL. The elution of Net-1+DCC long was similar to Net-1+DCC short. Net-1+DCC long eluted at 10.33 mL as a single peak.

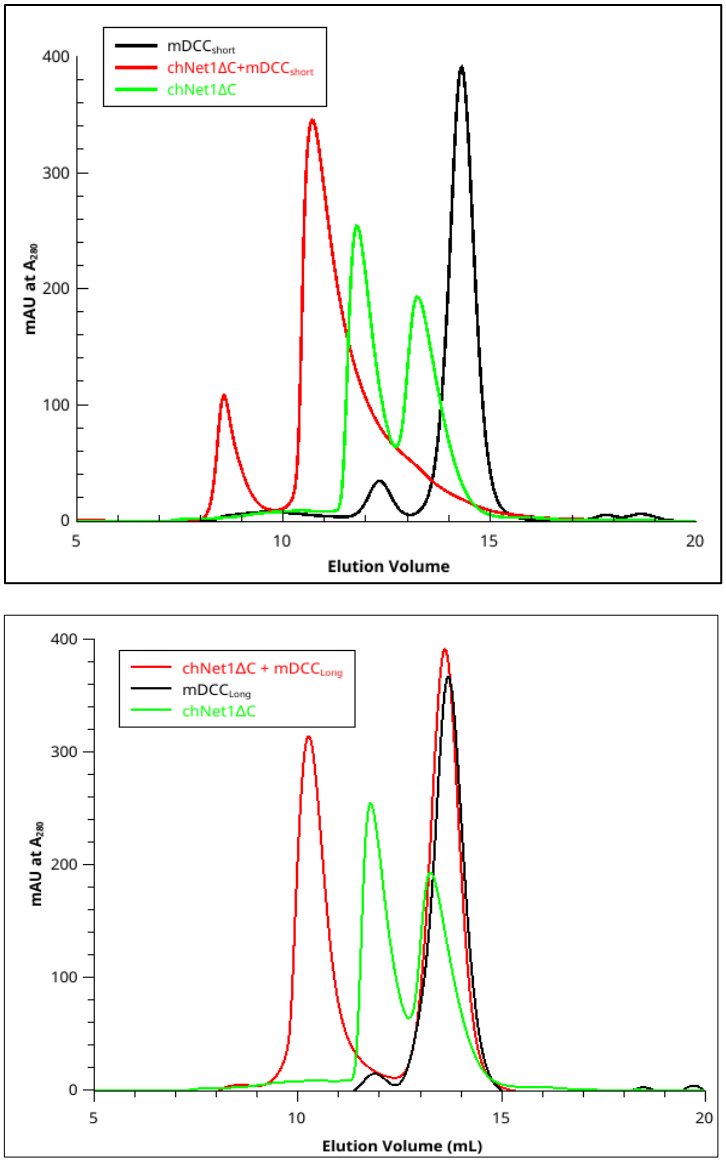

Figure 8: (A) SEC elution profiles of DCC short (black), Net1 (green) and Net-1+DCCshoort complex 1:1 molar ratio (red), (B) SEC elution profiles of DCC long (black), Net1 (green) and Net-1 + DCC long complex (red) 1:1 molar ratio. The profiles were acquired from the Superdex 200 10/300 GL size exclusion chromatography column.

Biological Small Angle X-ray Scattering

The pair wise (Pr) distribution gives information on the general shape and size of molecule measured. In this case the receptor and complex both had elongated and rod like shapes. the Kratky plot for proteins provides information of the overall shape and flexibility[42]. Change in flexibility in a protein after ligand binding shows that conformational change causes a change in flexibility. The Kratky plot (Figure 9C) suggests that DCC short (red)is a disordered protein and when interacting with Net-1 undergoes a stabilizing conformational change. The same is evident for DCC long and Net-1+DCC long, (Figure 10C) upon interaction, the receptor undergoes a change and becomes more stable. Due to the flexibility of the receptors, the dummy atom models and the density maps one of many possible conformations DCC short and DCC long take, but the χ^2 (Table 1) and the agreement of the models and maps to the experimental scattering suggest that the models and maps provide relevant information of the shapes and sizes of the proteins.

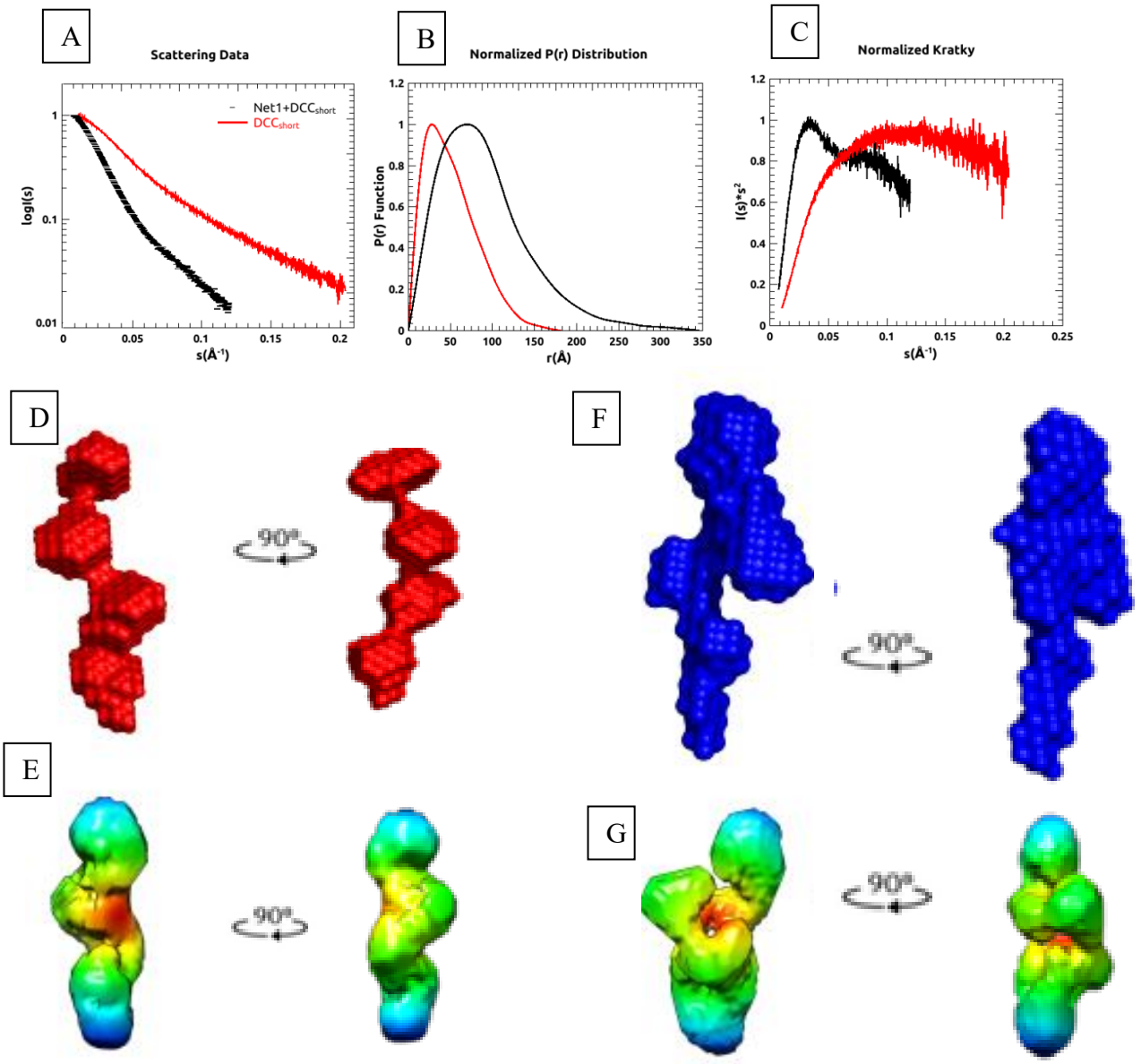

Figure 9: Solution conformation of DCC short and Net-1+DCC short determines by SAXS. A. Scattering profiles of DCC short (red) and Net-1+DCC short(black). The data was collected in 20 mM Tris, pH 7.5, 200 mM NaCl. B. Pair distribution functions for the receptor and complex. C. Normalized Kratky plot of the receptor and complex. D. Average low resolution DAMMIN representation of the DCC short (red), E. Electron density map of DCC short, F. Average low

resolution DAMMIN representation of the Net-1+DCC short (brown), G. Electron density map of Net-1+DCC short.

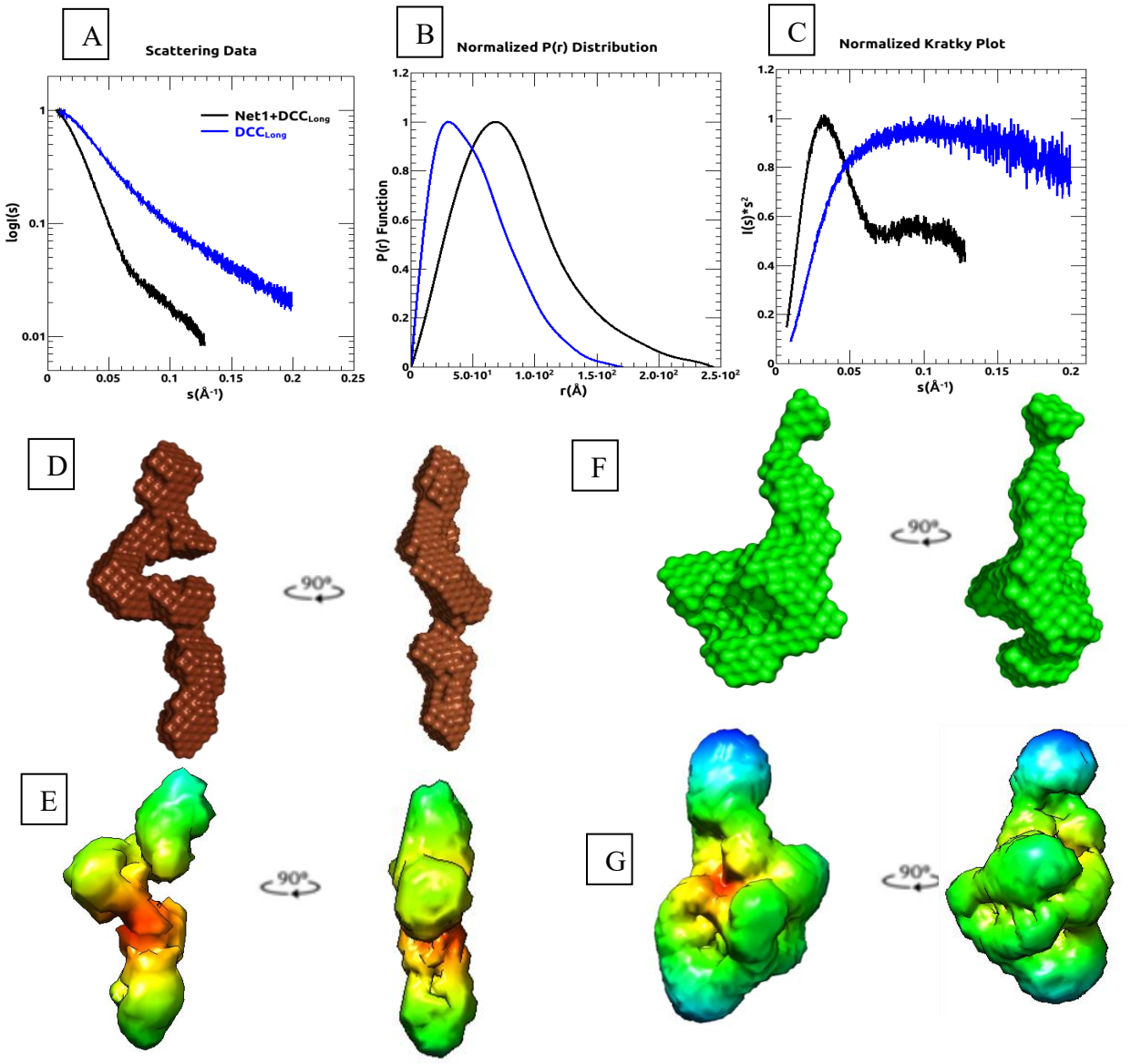

Figure 10: Solution conformation of DCC short and Net-1+DCC short determined by SAXS. A. Scattering profiles DCC long(blue) and Net-1+DCC long(black). The data was collected in 20 mM Tris, pH 7.5, 200 mM NaCl. B. Pair distribution functions for the receptor and complex. C. Normalized Kratky plot of the receptor and complex. D. Average low resolution DAMMIN representation of the DCC long (brown), E. Electron density map of DCC long, F. Average low

resolution DAMMIN representation of the Net-1+DCC long (green), G. Electron density map of

	Experimental data[a]		Dammin Models[c]			Denss Maps[d]		
	R_G (Å)	D_{max}(Å)[b]	R_G (Å)	D_{max}(Å)	χ_2	R_G (Å)	D_{max}(Å)	χ_2
Net-1+DCC long	65.69	243.5	65.84	251.1	1.160	63.21	245.77	0.129
Net-1+DCC short	72.86	295.0	72.99	284.0	1.098	65.56	228.1	0.221
DCC short	42.02	171	40.13	137.0	1.127	41.663	186.65	0.109
DCC long	47.77	170	42.24	154.9	1.087	41.459	146.85	0.294

Net-1+DCC long.

Table 1: Hydrodynamic data summary from SAXS data

[a] The values were experimentally determined from SAXS data obtained from P(r) analysis by GNOM

[b] D_{max} values obtained by ScÅtter and have 10-20% error rate.

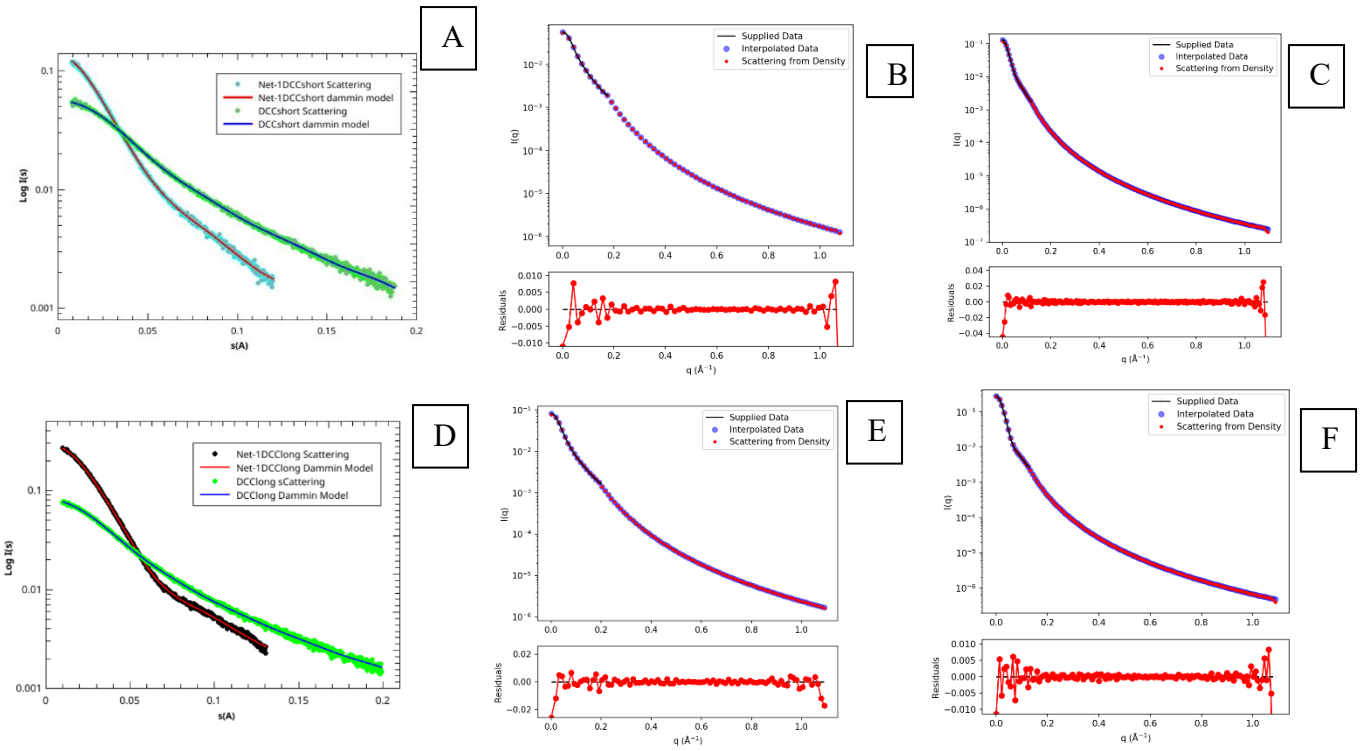

Figure 11: Dammin and Denss fitting results of refined models and maps. (A) Dammin fitting results for DCC short and Net-1+DCC short, (D) Dammin fitting results for DCC long and Net-1+DCC long. Denss map fit results of (B) DCC short, (C) Net-1+DCC short, (E) DCC long, (F) Net-1+DCC long

Analytical Ultracentrifugation

DCC short and DCC long were sedimented at 42,000 rpm for 24 hours at 20C, at 299nm and 287 nm. The sedimentation velocity data (figure 12) were analyzed using parametrically constrained spectrum analysis using a straight line function. DCC short and DCC long sedimented at 2.605 S and 2.718 S, which have associated molecular masses of 39.22kDa and 39.58kDa respectively. DCC short and DCC long had frictional ratios of 1.605 and 1.573 which mean that compared to a perfectly spherical object with the same size and density, the proteins will have 60.5% and 57.3% more friction as they sediment.

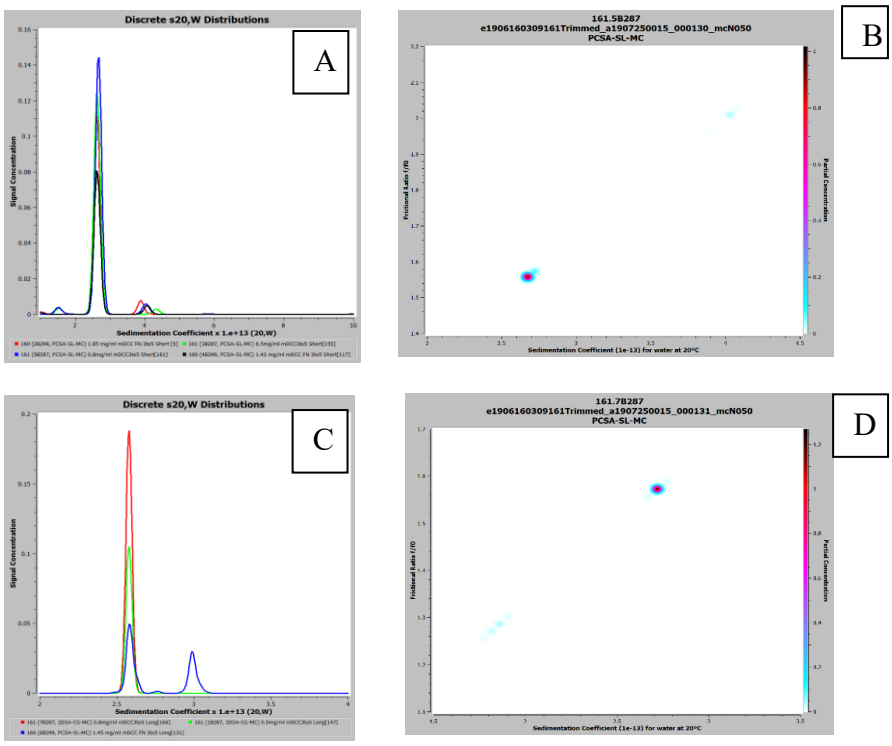

Figure 12: Sedimentation velosity distribution of (A)DCC short and (B) DCC long. Pseudo-3D distribution of sedimentation and fractional ratio of (C)DCC short and (D) DCC long.

Table 2: AUC sedimentation velocity data summary of DCC short and DCC long.

	Molecular Mass (kDa)	Sedimentation coefficient (10^{-13} S)	f/f_0 Ratio	Diffusion coefficient
DCC short	39.22	2.605	1.605	$5.970e^{-7}$
DCC long	39.58	2.718	1.573	$6.226e^{-7}$

X-ray Crystallography

The crystal structure, currently in refinement, was built using coot and phased using PDB code 4PLO and 2ED9 (to be published). The structure shows an asymmetric unit of dimeric DCC short binding in an antiparallel fashion two FN III 4 domains with two FNIII 5 domains. The FNIII 3 domains in the crystal made crystal contact with other asymmetric units. (Figure 14). The biological assembly as suggested by the AUC and SEC results may be the monomeric DCC and that the dimerization may be an artifact of crystal packing.

Table 3: Crystallization trial solutions that produced protein crystals.

Protein	Concentration (mg/mL)	Screen	Condition
DCC short	13.25	JBS Classic 1-4	25% w/v Polyethylene Glycol (PEG) 4000, 100 mM TRIS pH 8.5, 200 mM Calcium chloride
DCC short	13.25	JBS Classic 1-4	10% w/v PEG 8000, 100 mM HEPES pH 7.5, 200 mM Calcium Acetate
DCC short	13.25	JCSG ++1 - ++4	40% MPD, 5% w/v PEG 8000, 100 mM MES pH 6.5
DCC short	13.25	Index	200 mM Calcium chloride dihydrate, 100 mM Bis-TRIS pH 5.5, 40% MPD
Net-1+ DCC short	12.39	Netrix	0.01M Magnesium chloride hexahydrate, 0.05 MES monohydrate pH5.6, 1.8 Lithium Sulfate monohydrate
Net-1+ DCC short	12.39	Netrix	0.002M Calcium Chloride dihydrate 0.05 Sodium Cocadylate trihydrate pH 6, 1.8 Ammonium Sulfate, 0.0005 Spermine
Net-1+ DCC short	12.39	JBS Classic 5-8	1.6M Ammonium Sulfate, 500 mM Lithium Chloride
Net-1+ DCC short	12.39	JBS Classic 5-8	1.8M Ammonium Sulfate, 100 mM MES pH 6.5
Net-1+ DCC long	10.55	Index	0.2M Ammonium Sulfate, 100 mM HEPES pH 7.5, 45% MPD
Net-1+ DCC long	10.55	JBS Classic 1-4	5% w/v PEG 4000, 100 mM MES pH 6.5, 200 mM Magnesium Chloride
Net-1+ DCC long	10.55	JBS Classic 1-4	25% w/v PEG 4000, 100 mM TRIS pH 8.5, 200 mM Calcium chloride

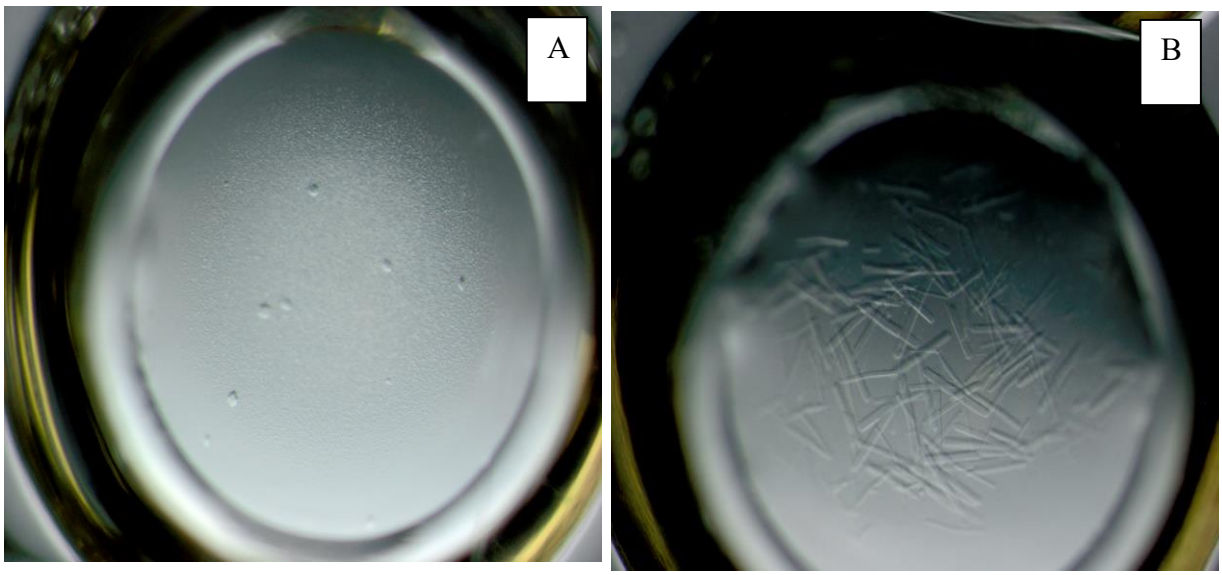

Figure 13: Images of crystals of (A) DCC short and (B) Net-1+DCC short. Crystals were grown by vapour diffusion in A) 25% w/v Polyethylene Glycol (PEG) 4000, 100 mM TRIS pH 8.5, 200 mM calcium chloride and B) 1.8M ammonium sulfate, 100 mM MES pH 6.5. sitting drops were prepared by adding 0.6 µL of reservoir solution to 0.6 µL of protein at 13.25 mg/mL and 12.29 mg/mL DCC short and Net-1+DCC short complex.

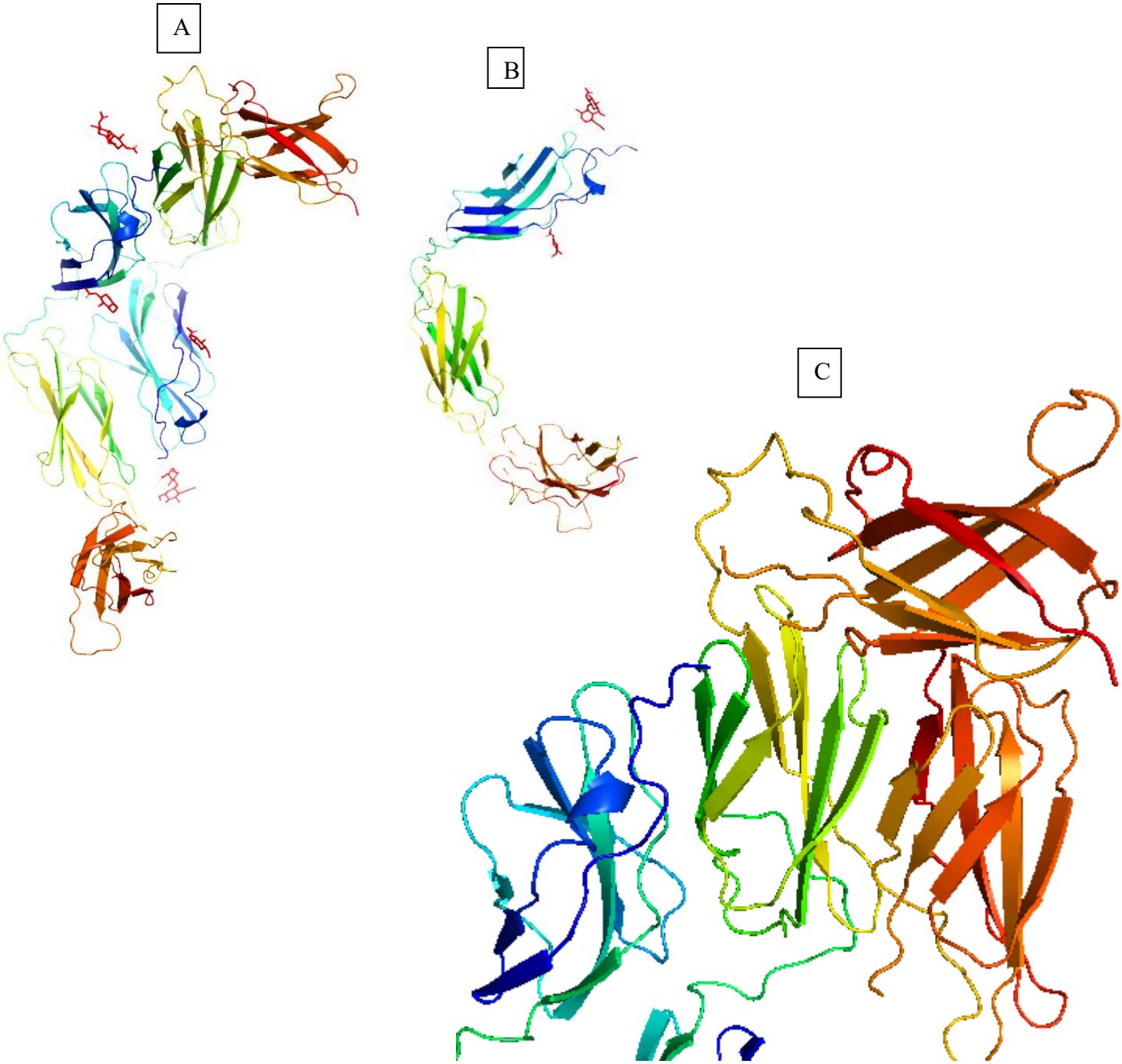

Figure 14: Figure 1. Overall Structure of DCC short ribbon model. (A) Dimer DCC short and (B) Monomeric DCC short. The domains FNIII 3 (red), FNIII 4 (green yellow), and FNIII 5 (blue) colored accordingly. N-linked glycans are drawn as red sticks. (C) Close up of FN III 3(red/orange) interacting with a crystal mate.

Table 4: Data collection, phasing and refinement summary of structure in figure 14

Data Collection	Overall
Wavelength	1.03317
Resolution	2.59
Rmeas	0.088
Rpim	0.04
Space group	$P2_1\ 2_1\ 2_1$
Cell dimensions	49.52 97.95 124.05 90.00 90.00 90.00

Phasing	
Figure of merit	0.76

Refinement	
Resolution	2.99
Number of Reflections	27910
R/Rfree	0.2641/0.2253
Overall CC	0.807

Mean B-factor	
Protein	70.42
Glycans at Asns	135.64
Rmsd	
Bond length	0.01
Bond angle	1.285

Ramachandran	(%)
Favoured	87.54
Allowed	8.48
Disallowed	3.98

Discussion

Dimerization of DCC short and DCC long

To analyze DCC short and DCC long which has an additional 20 amino acid linker, a number of techniques were used, including size exclusion chromatography, analytical ultracentrifugation, biological small angle X-ray scattering and X-ray crystallography.

For SEC elution run, the receptors were prepared in 50 mM tris pH 7.5, 200 mM NaCl and purified on a 25 mL Superdex 200 10/300 column. DCC short eluted as 2 peaks at 13.17 mL and at 14.28 mL (Figure 8A, black), while DCC long eluted only at 13.72 mL (Figure 8B black). The SEC profile showed that DCC short exists as two or more species and DCC long exists as a single species. Netrin-1 showed a similar elution profile as DCC short, 2 peaks at 11.77 mL and 13.26 mL elution volume (figure 8A green). From previous unpublished studies, it was known Netrin-1 exists in a monomer-dimer equilibrium. Though there is no direct correlation between the size of the particle and the elution volume, the shape also influences how the particle travels down and through the Superdex column, it likely that DCC short and long are predominantly monomers.

During the AUC experiments, concentrations 0.2, 0.5, 1.43 and 1.85 mg/mL of DCC short and 0.2, 0.5, 1.45 mg/mL DCC long were sedimented at 42,000 rpm for 24 hours at 20C. Concentrations greater then 0.8 were measured at at 299nm and concentration equal to or lower than 0.8 mg/mL were measured at 287 nm. Th method allowed measurements of concentrations outside the linearly observable ranges in the Bachman Coulter Optima XLI instrument, as well as determine if DCC short and long self associated at concentrations described. The sedimentation velocity data (figure 11) were analyzed using parametrically

constrained spectrum analysis using a straight-line function by Ultrascan III. The masses calculated for DCC short and DCC long were 39.22kDa and 39.58kDa respectively. DCC short and DCC long had fractional ratios of 1.605 and 1.573 which mean that compared to a perfectly spherical object with the same size and density, the proteins will have 60.5% and 57.3% more friction as they sediment. Compared to the sequenced based masses, 37.67 kDa DCC short and 38.75 kDa DCC long, the measured values are much bigger possible due to N-linked glycosylation that occurred.

The pair we (Pr) distribution and the Kratky plot show that both DCC short and long are long flexible rod like proteins with for proteins provides information of the overall shape and flexibility[43]. They are both of similar sizes, Radius of Gyration of 42.02 Å and 47.77 Å DCC short and DCC long respectively from the experimental data. Similar results are given for the DAMMIN and Denss models (Table 1). Unfortunately, because the receptors are very flexible the models generated by DAMMIN and Denss are an average of all the conformations present in the solution at the time of scattering, not necessarily the accurate depiction of DCC short or DCC long. In addition, during shipment, the extremely concentrations they were sent at may affect the behaviour of the samples as the eluted the size exclusion column and scattered. For these reasons, the Bio-SAXS results should only be considered qualitative not quantitative. The χ^2 (Table 1), the agreement of the models and maps to the experimental scattering (Figure 11 A, B, C and E) and the crystal structure suggested that the models and maps provided relevant information of the shapes and sizes of the proteins (Figure 16).

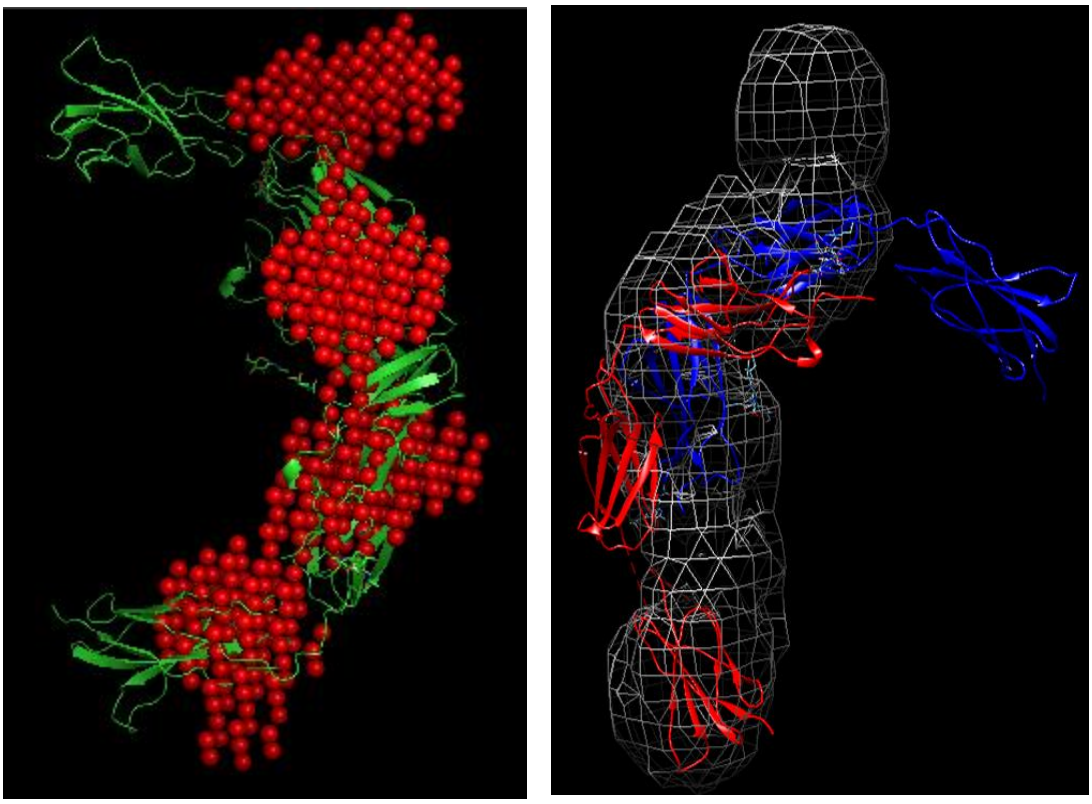

Figure 15: overlap of DCC short crystal structure with (A) DAMMIN model and (B) Denss map

The asymmetric unit, the smallest unit of repeat to make the unit cell, was a dimeric DCC short. While the structure currently in refinement, when compared to the Bio-SAXS result, both confirmed that DCC can be a dimer and showed the interface of dimerization. DCC short units bounded in an anti-parallel orientation where FN III 4 of one protein bonded to the FN III 5 of another. Th formed a four-domain core with FN III 3 of both units freely moving in solution. In the crystal structure FN III 3 formed the crystal contact to the next asymmetric unit with FN III 4 (Figure 14). When compared to the models generated by DAMMIN and Denss (Figure 15), the crystal structure aligned except for one FN III 3, when considered how flexibility DCC short was.

Netrin-1 + DCC short and Netrin-1 + DCC complexes

To characterize how the DCC receptors interacted with Netrin-1, the complexes were analyzed with the same techniques as for DCC characterization. In the SEC profiles Net-1+DCC short eluted as two peaks at 8.68 mL and 10.64 mL. The 10.64 mL peak was skewed to the right which likely due to a small excess of Netrin-1 or DCC short, and the 8.68 mL peak was due to aggregation since it eluted in the void volume of the column.

Upon binding to Net-1, the flexible DCC short and DCC long was reduced and the formed a stable complex as show in the Kratky plot. The P(r) distributions also showed that both Net-1+DCC short and Net-1+DCC long are long extended molecules. Since the complexes are stable, the models and maps generated by DAMMIN and Denss can be used depict the low-resolution structures of the complexes.

Both Denss and DAMMIN were used in the analysis of Net-1+DCC short and Net-1+DCC long first, because both programs have different methods of generating models based on the experimental scattering data. The models generated can be verified by if they are generating by different methods from the same experimental data. Secondly, Denss, a new method that more computationally effective and generated a model in a portion of the time used by DAMMIN. If Denss constantly generates models that are representative of the data, then it can be the main Bio-SAXS analysis tool in the Stetefeld laboratory.

For Net-1+DCC short and Net-1+DCC long, both Denss and DAMMIN gave similar models (Figure 9D-G, Figure 10 D-G). The radius of gyration and Dmax of both denss and DAMMIN were consistent with the experimental data. The goodness of fit for denss was much lower since

denss is better able to fit noise from the solution, while DAMMIN assigns bead with the same radius and density as the protein model to the solution. Even with a reduced fit to the buffer solution, DAMMIN models fit well with the experimental data (Figure 11A, B).

AUC experiments of Net-1+DCC short and Net-1+DCC long were conducted but sizable aggregation made analysis uninterpretable and have been excluded from the report. Both Net-1+DCC short and Net-1+DCC long had conditions with sizable crystal growth (Table 2, Figure 14B), but due to poor diffraction, no structure of the complexes has been built.

Conclusion

Netrin-1 and DCC are involved in the guidance of several axons in the central and peripheral nervous systems, in addition, as a function of DCC as a dependence receptor, it considered a tumour suppressor and Netrin-1 an oncogenic gene. For these reasons, it is important to understand how they interact with each other and the downstream effects of their interactions.

DCC as a dependence receptor signals cells when to initiate apoptosis, programmed cell death, in the absence of Netrin-1. Based on results from DCC short, a hypothesis is that apoptosis signalled by a monomeric DCC and survival factor signalled by dimeric DCC, since DCC short does not seem to be dimeric in solution. netrin-1 binding allows for DCC dimerization more readily and a survival signal can be propagated. Since DCC is a single transmembrane helix receptor, binding in the extracellular domain cannot propagate a signal downstream without dimerization.

The hypothesis requires more then one Net-1+DCC binding site to occur which can mean more then one targets for cancer treatments, as developments in drugs against protein-protein interactions making headway.

Future Aims

To understand how Net-1+DCC short and Net-1+DCC long interact, high resolution structures, under different conditions then determined by Finci et al[28,29], are required. In addition, an AUC experiment with milt-wavelength analysis of fluorescent tags fused DCC short, DCC long and Net-1 will be conducted to determine the stoichiometry of Net-1+DCC short and Net-1+DCC long. The equilibrium constant of complex formations and self-association of Net-

1+DCC and DCC respectively can be determined using this method of AUC experiment. To verify the BIO-SAXS results, scattering experiments with varied concentrations of the complexes will be completed to reduce effect of shifting concentration on the samples as they are shipped.

References

[1] Stoeckli, Esther T. "**Understanding Axon Guidance: Are We Nearly There Yet**?" *Development* 145, no. 10 (May 15, 2018): dev151415. https://doi.org/10.1242/dev.151415.

[2]Berzat, A.; Hall, A. **Cellular Responses to Extracellular Guidance Cues**. *EMBO J* 2010, *29* (16), 2734–2745. https://doi.org/10.1038/emboj.2010.170.

[3] Ahmed, G., Shinmyo, Y., Ohta, K., Islam, S.M., Hossain, M., Naser, I.B., Riyadh, M.A., Su, Y., Zhang, S., Tessier-Lavigne, M.*, et al.* (2011). **Draxin inhibits axonal outgrowth through the netrin receptor DCC. The Journal of neuroscience** : the official journal of the Society for Neuroscience *31*, 14018-14023.

[4] ursky, S.L., and Sanes, J.R. (2010). **Chemoaffinity revisited: dscams, protocadherins, and neural circuit assembly**. Cell *143*, 343-353.

[5] Lowery, Laura Anne, and David Van Vactor. **The Trip of the Tip: Understanding the Growth Cone Machinery.** *Nature Reviews. Molecular Cell Biology* 10, no. 5 (May 2009): 332–43. https://doi.org/10.1038/nrm2679.

[6] Alberts, Bruce, Alexander Johnson, Julian Lewis, Martin Raff, Keith Roberts, and Peter Walter. "**Neural Development.**" ***Molecular Biology of the Cell****. 4th Edition*, 2002. https://www.ncbi.nlm.nih.gov/books/NBK26814/.

[7] Schaefer, F.W., Kabir, N., Forscher, P., **Filopodia and Actin Arcs Guide the Assembly and Transport of Two Populations of Microtubules with Unique Dynamic Parameters in Neuronal Growth Cones** | JCB." http://jcb.rupress.org/content/158/1/139.full.

[8] Plachez, Céline, and Linda J. Richards. "**Mechanisms of Axon Guidance in the Developing Nervous System.**" In *Current Topics in Developmental Biology*, 69:267–346. Neural Development. Academic Press, 2005. https://doi.org/10.1016/S0070-2153(05)69010-2.

[9] Chan, S.S., Zheng, H., Su, M.W., Wilk, R., Killeen, M.T., Hedgecock, E.M., and Culotti, J.G. (1996). **UNC-40, a C. elegans homolog of DCC (Deleted in Colorectal Cancer), is required in motile cells responding to UNC-6 netrin cues**. Cell *87*, 187-195.

[10] Grandin M., Meier M., Delcros J. G., et al. **Structural decoding of the Netrin-1/UNC5 interaction and its therapeutical implications in cancers**. *Cancer Cell*. 2016;29(2):173–185.

[11] Lai Wing Sun K, Correia JP, Kennedy TE. **Netrins: versatile extracellular cues with diverse functions**. Dev. Camb. Engl. 2011;138:2153–2169.

[12] Rajasekharan S, Kennedy TE. **The netrin protein family**. Genome Biol. 2009;10:239.

[13] Reuten, Raphael, Trushar R. Patel, Matthew McDougall, Nicolas Rama, Denise Nikodemus, Benjamin Gibert, Jean-Guy Delcros, et al. **Structural Decoding of Netrin-4 Reveals a**

Regulatory Function towards Mature Basement Membranes. *Nature Communications* 7 (30 2016): 13515. https://doi.org/10.1038/ncomms13515.

[14] Ly A, Nikolaev A, Suresh G, Zheng Y, Tessier-Lavigne M, Stein E. D**SCAM is a netrin receptor that collaborates with DCC in mediating turning responses to netrin-1**. Cell. 2008;133:1241–1254.

[15] Krimpenfort P, Song J-Y, Proost N, Zevenhoven J, Jonkers J, Berns A. **Deleted in colorectal carcinoma suppresses metastasis in p53-deficient mammary tumours**. Nature. 2012;482:538–541.

[16] Mazelin L, Bernet A, Bonod-Bidaud C, Pays L, Arnaud S, Gespach C, Bredesen DE, Scoazec J-Y, Mehlen P. **Netrin-1 controls colorectal tumorigenesis by regulating apoptosis**. Nature. 2004;431:80–84.

[17] Keino-Masu K, Masu M, Hinck L, Leonardo ED, Chan SS, Culotti JG, Tessier-Lavigne M. **Deleted in Colorectal Cancer (DCC) encodes a netrin receptor**. Cell. 1996;87:175–185

[18] Chen Q, Sun X, Zhou X, Liu J, Wu J, Zhang Y, Wang J. **N-terminal horseshoe conformation of DCC is functionally required for axon guidance and might be shared by other neural receptors**. J. Cell Sci. 2013;126:186–195.

[19] Wilson NH, Key B. **Neogenin interacts with RGMa and netrin-1 to guide axons within the embryonic vertebrate forebrain.** Dev. Biol. 2006;296:485–498.

[20] Colamarino SA, Tessier-Lavigne M. T**he axonal chemoattractant netrin-1 is also a chemorepellent for trochlear motor axons**. Cell. 1995;81:621–629

[21] Geisbrecht, B.V., Dowd, K.A., Barfield, R.W., Longo, P.A., and Leahy, D.J. (2003). **Netrin binds discrete subdomains of DCC and UNC5 and mediates interactions between DCC and heparin**. The Journal of biological chemistry *278*, 32561-32568.

[22] Andrews GL, Tanglao S, Farmer WT, Morin S, Brotman S, Berberoglu MA, Price H, Fernandez GC, Mastick GS, Charron F, et al. **Dscam guides embryonic axons by Netrin-dependent and -independent functions**. Dev. Camb. Engl. 2008;135:3839–3848.

[23] Liu G, Li W, Wang L, Kar A, Guan K-L, Rao Y, Wu JY. D**SCAM functions as a netrin receptor in commissural axon pathfinding**. Proc. Natl. Acad. Sci. U. S. A. 2009;106:2951–2956.

[24] Fitamant, Julien, Céline Guenebeaud, Marie-May Coissieux, Catherine Guix, Isabelle Treilleux, Jean-Yves Scoazec, Thomas Bachelot, Agnès Bernet, and Patrick Mehlen. **Netrin-1 Expression Confers a Selective Advantage for Tumor Cell Survival in Metastatic Breast Cancer**. *Proceedings of the National Academy of Sciences of the United States of America* 105, no. 12 (March 25, 2008): 4850–55. https://doi.org/10.1073/pnas.0709810105.

[25]Meyerhardt, J. A., K. Caca, B. C. Eckstrand, G. Hu, C. Lengauer, S. Banavali, A. T. Look, and E. R. Fearon. "**Netrin-1: Interaction with Deleted in Colorectal Cancer (DCC) and Alterations in Brain Tumors and Neuroblastomas**." *Cell Growth & Differentiation: The Molecular Biology Journal of the American Association for Cancer Research* 10, no. 1 (January 1999): 35–42.

[26] Shin, Sung Kwan, et al. "**Epigenetic and Genetic Alterations in Netrin-1 Receptors UNC5C and DCC in Human Colon Cancer**." *Gastroenterology*, vol. 133, no. 6, Dec. 2007, pp. 1849–1857,

[27] Grady, W.M. (2007). **Making the Case for DCC and UNC5C as Tumor-Suppressor Genes in the Colon. *Gastroenterology***, 133(6), pp.2045–2049.

[28] Finci, L., et al. "**Signaling Mechanism of the Netrin-1 Receptor DCC in Axon Guidance**." *Progress in Biophysics and Molecular Biology*, vol. 118, no. 3, Sept. 2015, pp. 153–160, 10.1016/j.pbiomolbio.2015.04.001.

[29] Finci, Lorenzo I., et al. "**The Crystal Structure of Netrin-1 in Complex with DCC Reveals the Bifunctionality of Netrin-1 As a Guidance Cue**." *Neuron*, vol. 83, no. 4, Aug. 2014, pp. 839–849, 10.1016/j.neuron.2014.07.010.

[30] Schuck, P. (2013) **Analytical Ultracentrifugation as a Tool for Studying Protein Interactions**. Biophys. Rev.

[31]Colfen, Helmut, and Colfen, Helmut. **Analytical Ultracentrifugation.** *Macromolecular Bioscience* 10.7 (2010): 687–688. Web.

[32] Cole, J. L., Lary, J. W., Moody, T., and Laue, T. M. (2009) **Analytical Ultracentrifugation: Sedimentation Velocity and Sedimentation Equilibrium.** Methods Cell Biol. 84, 1433–17

[33] Demeler B, Brookes E, Wang R, Schirf V, Kim CA. **Characterization of Reversible Associations by Sedimentation Velocity with UltraScan**. Macromol. Biosci. 2010. 10(7):775-82.

[34] Gorbet, Gary, Taylor Devlin, Blanca I. Hernandez Uribe, Aysha K. Demeler, Zachary L. Lindsey, Suma Ganji, Sabrah Breton, et al. "**A Parametrically Constrained Optimization Method for Fitting Sedimentation Velocity Experiments**." *Biophysical Journal* 106, no. 8 (April 15, 2014): 1741–50. https://doi.org/10.1016/j.bpj.2014.02.022.

[35] Semenyuk, A., and Svergun, D. I. (1991) **GNOM - a program package for small-angle scattering data processing**. J. Appl. Crystallogr. 24, 537–540

[36] Franke, D., M. V. Petoukhov, P. V. Konarev, A. Panjkovich, A. Tuukkanen, H. D. T. Mertens, A. G. Kikhney, et al. "***ATSAS 2.8* : A Comprehensive Data Analysis Suite for Small-Angle Scattering from Macromolecular Solutions**." *Journal of Applied Crystallography* 50, no. 4 (August 1, 2017): 1212–25. https://doi.org/10.1107/S1600576717007786.

[37] Franke, D., and Svergun, D. I. (2009) **DAMMIF, a program for rapid ab-initio shape determination in small-angle scattering**. J. Appl. Crystallogr. 42, 342–346

[38] Grant, Thomas D. "***Ab Initio* Electron Density Determination Directly from Solution Scattering Data.**" *Nature Methods* 15, no. 3 (March 2018): 191–93. https://doi.org/10.1038/nmeth.4581.a

[39] Owski, Zbyszek, and Wladek Minor. "[20] **Processing of X-Ray Diffraction Data Collected in Oscillation Mode**." *Methods in Enzymology*, 1997, pp. 307–326,

[40] Collaborative Computational Project, Number 4. "**The CCP4 Suite: Programs for Protein Crystallography**." *Acta Crystallographica. Section D, Biological Crystallography*, vol. 50, no. Pt 5, 1994, pp. 760–3.

[41] Emsley, P., B. Lohkamp, W. G. Scott, and K. Cowtan. "**Features and Development of Coot**." *Acta Crystallographica. Section D, Biological Crystallography* 66, no. Pt 4 (April 2010): 486–501. https://doi.org/10.1107/S0907444910007493.

[42] Kratky, O., and Porod, G. (1949) **Roetgenuntersuchung Geloester Fadenmolekuele**. Recl. des Trav. Chim. des Pays-Bas. 68, 1106–1122